Structural Analysis of Glyceraldehyde 3-Phosphate Dehydrogenase from *Escherichia coli*: Direct Evidence of Substrate Binding and Cofactor-Induced Conformational Changes[†,‡]

Mikyung Yun, Cheon-Gil Park, Ji-Yeon Kim, and Hee-Won Park*

Department of Structural Biology, St. Jude Children's Research Hospital, 332 North Lauderdale, Memphis, Tennessee 38105

Received November 24, 1999; Revised Manuscript Received June 23, 2000

ABSTRACT: The crystal structures of gyceraldehyde 3-phosphate dehydrogenase (GAPDH) from *Escherichia coli* have been determined in three different enzymatic states, NAD^+-free, NAD^+-bound, and hemiacetal intermediate. The NAD^+-free structure reported here has been determined from monoclinic and tetragonal crystal forms. The conformational changes in GAPDH induced by cofactor binding are limited to the residues that bind the adenine moiety of NAD^+. Glyceraldehyde 3-phosphate (GAP), the substrate of GAPDH, binds to the enzyme with its C3 phosphate in a hydrophilic pocket, called the "new P_i" site, which is different from the originally proposed binding site for inorganic phosphate. This observed location of the C3 phosphate is consistent with the flip-flop model proposed for the enzyme mechanism [Skarzynski, T., Moody, P. C., and Wonacott, A. J. (1987) *J. Mol. Biol. 193*, 171−187]. Via incorporation of the new P_i site in this model, it is now proposed that the C3 phosphate of GAP initially binds at the new P_i site and then flips to the P_s site before hydride transfer. A superposition of NAD^+-bound and hemiacetal intermediate structures reveals an interaction between the hydroxyl oxygen at the hemiacetal C1 of GAP and the nicotinamide ring. This finding suggests that the cofactor NAD^+ may stabilize the transition state oxyanion of the hemiacetal intermediate in support of the flip-flop model for GAP binding.

GAPDH[1] is an enzyme essential for glycolysis in both prokaryotes and eukaryotes. This enzyme functions as a homotetramer with a molecular mass of approximately 150 kDa, and catalyzes the oxidative phosphorylation of glyceraldehyde 3-phosphate (GAP) to 1,3-bisphosphoglycerate (BPG) using the cofactor NAD^+. The first reaction step involves the formation of a hemiacetal intermediate between GAP and a cysteine residue, and this hemiacetal intermediate is then oxidized to a thioester, with concomitant reduction of NAD^+ to NADH. The reduced NADH is then exchanged with the second NAD^+, and the thioester is attacked by a nucleophilic inorganic phosphate to produce BPG (*1*).

The crystal structures of NAD^+-bound GAPDH (holoenzyme) have been determined at different resolutions from various organisms, including the American lobster (*2*), the Chinese lobster (*3*, *4*), humans (*5*), *Bacillus stearothermophilus* (*6*), *Thermotoga maritima* (*7*), *Thermus aquaticus* (*8*), *Escherichia coli* (*9*), *Leishmania mexicana* (*10*, *11*), *Trypanosoma brucei* (*12*, *13*), and *Trypanosoma cruzi* (*14*). The structures of NAD^+-free GAPDH (apoenzyme) have been determined from the American lobster at low resolution (*15*), and at high resolution from the thermophiles *B. stearothermophilus* (*16*) and *Sulfolobus solfataricus* (*17*). A structural comparison of the apoenzyme and the holoenzyme from *B. stearothermophilus* has revealed that a conformational change of the protein is induced by NAD^+ binding. The conformational change includes relative shifts of several structural elements in the coenzyme-binding domain, and some small movements in the catalytic domain (*16*).

Here we describe the structures of apo-GAPDH and holo-GAPDH from *E. coli* in monoclinic crystal forms at a resolution of 2.0 Å. This monoclinic apoenzyme structure is the first high-resolution model of ligand-free GAPDH from a mesophilic organism. We present a detailed analysis of the differences between the monoclinic apoenzyme and holoenzyme structures. We also report the 2.5 Å structure of a tetragonal form of the complex of *E. coli* GAPDH that contains the hemiacetal intermediate of GAP bound to the active site. This structure shows that the C3 phosphate of GAP binds at a new P_i site, which is different from the originally proposed binding site for inorganic phosphate (*2*). This finding supports the flip-flop model as the mode of GAP binding. Finally, the superposition of the structures of the holoenzyme and the hemiacetal enzyme leads us to propose that the cofactor NAD^+ may stabilize the transition state

[†] Supported in part by NIH Cancer Center Support Grant P30 CA21765 and by the American Lebanese Syrian Associated Charities.

[‡] The structure factors and coordinates have been deposited with the Protein Data Bank with accession codes 1dc3, 1dc4, 1dc5, and 1dc6.

* To whom correspondence should be addressed: Department of Structural Biology, St. Jude Children's Research Hospital, 332 N. Lauderdale, Memphis, TN 38105. Lab: (901) 495-3839. Office: (901) 495-3838. Fax: (901) 495-3032. E-mail: hee-won.park@stjude.org.

[1] Abbreviations: BPG, 1,3-bisphosphoglycerate; D-GAP, D stereoisomer of GAP; DTT, dithiothreitol; EDTA, ethylenediaminetetraacetic acid; FPLC, fast protein liquid chromatography; GAP, glyceraldehyde 3-phosphate; GAPDH, glyceraldehyde 3-phosphate dehydrogenase; L-GAP, L stereoisomer of GAP; MAD, multiwavelength anomalous dispersion; NAD^+, nicotinamide adenine dinucleotide (oxidized form); NADH, nicotinamide adenine dinucleotide (reduced form); NCS, noncrystallographic symmetry; NSLS, National Synchrotron Light Source; PEG, polyethylene glycol; PMSF, phenylmethanesulfonyl fluoride; rms, root-mean-square; Se-Met, selenomethionine.

10.1021/bi9927080 CCC: $19.00
Published on Web 08/11/2000

Table 1: Data Collection Statistics

	tetragonal crystal forms				monoclinic crystal forms	
	apoenzyme					
	inflection	peak	remote	hemiacetal enzyme	apoenzyme	holoenzyme
wavelength (Å)	0.9792	0.9785	0.9641	1.54	1.54	1.54
resolution (Å)	20−2.5	20−2.5	20−2.5	20−2.5	20−2.0	20−1.9
no. of reflections						
measured	1055831	2194523	1004647	299063	498853	660366
unique	38253	38250	31502	38926	44636	51859
completeness (%, $>-3\sigma$)						
overall	99.8	99.8	82.5	99.8	93.5	91.4
last shell	100.0	100.0	84.2	99.9	73.9	48.1
R_{sym}[a] (%)	3.6	3.8	3.5	5.8	7.0	6.0
average $I/\sigma I$	14.5	16.0	13.9	13.9	11.0	10.3
anomalous scattering factors						
f' values	−8.26	−6.29	−3.26	−	−	−
f'' values	3.15	3.97	3.60	−	−	−

[a] $R_{sym} = \Sigma_{hkl}[\Sigma_i|I_{hkl,i} - \langle I_{hkl}\rangle|]/\Sigma_{hkl,i}\langle I_{hkl}\rangle$, where $I_{hkl,i}$ is the intensity of an individual measurement of the reflection with Miller indices *h*, *k*, and *l* and $\langle I_{hkl}\rangle$ is the mean intensity of that reflection.

oxyanion of the hemiacetal intermediate by means of a charge interaction.

EXPERIMENTAL PROCEDURES

Cell Culture and Purification. Methionine-auxotrophic cells from *E. coli* strain B834 (DE3) were grown in M9 medium supplemented with selenomethionine (Se-Met) for 15 h at 22 °C. The cells were harvested by centrifugation at 5000*g* and resuspended in 400 mL of the lysis buffer containing 20 mM Tris-HCl (pH 8.0), 1 mM DTT, 1 mM EDTA, and 1 mM PMSF. The resuspended cells were lysed by sonication, and the cell lysate was centrifuged at 14000*g* for 30 min. The GAPDH was purified from the supernatant by Q-Sepharose anion exchange chromatography. Eluted fractions containing GAPDH were pooled and concentrated. The concentrated sample was then further purified by filtration through a S-200 Superdex gel filtration column (Pharmacia) attached to a FPLC system (Pharmacia). The elution buffer for gel filtration contained 20 mM Tris-HCl (pH 7.6), 200 mM NaCl, 1 mM DTT, and 1 mM EDTA and was used at a flow rate of 60 mL/h. Fractions containing GAPDH, as confirmed by SDS−PAGE, were pooled. The final protein concentration in the elution buffer was 20 mg/mL.

Crystallization. The hanging-drop vapor-diffusion method was used to grow the Se-Met crystals of GAPDH. Hanging drops containing equal volumes of the protein solution and a reservoir solution were equilibrated at 18 °C against the reservoir solution [15% PEG 4000, 0.8−0.9 M $MgCl_2$, and 0.1 M Tris-HCl (pH 8.5)]. Two crystal forms, monoclinic and tetragonal, grew within 1 week. Both crystal forms were free of NAD^+ and GAP. The monoclinic form was called monoclinic apoenzyme crystals, and the tetragonal form was called tetragonal apoenzyme crystals. Fully grown crystals were transferred to a stabilization solution containing 20% PEG 4000, 0.9 M $MgCl_2$, 5 mM DTT, and 0.1 M Tris-HCl (pH 8.5). Crystals of NAD^+-bound enzyme, called holoenzyme crystals, were obtained by soaking the monoclinic apoenzyme crystals for 1 day in the stabilization solution to which 2 mM NAD^+ had been added. To obtain crystals of the hemiacetal enzyme, the crystals of the tetragonal apoenzyme were soaked in the $MgCl_2$-free stabilization solution to which 4 mM racemic GAP had been added. All crystals were flash-frozen in liquid nitrogen by using glycerol or PEG 400 as a cryoprotectant.

Data Collection. Multiwavelength anomalous dispersion (MAD) diffraction data were determined from a single Se-Met crystal of the tetragonal apo-GAPDH on beamline X9B at the National Synchrotron Light Source (NSLS), Brookhaven National Laboratory (Upton, NY). The detector was a Q4 CCD system (Brandeis) operating at 100 K. Before data collection was started, the X-ray absorption fluorescence spectrum of the Se-Met crystals was collected to accurately determine the variation of the anomalous signal as a function of wavelength. Using this spectrum, it was possible to precisely select the three wavelengths for data collection corresponding to (a) the inflection point of the selenium edge, (b) the peak of the selenium edge, and (c) a point above the edge at a remote shorter wavelength (high-energy remote). The data sets were integrated using the program HKL (*18*). Complete diffraction data for crystals of the hemiacetal enzyme and crystals of the monoclinic apoenzymes and holoenzymes were recorded with a DIP2030 system using a Cu rotating anode generator (Nonius) at 100 K. These data sets were processed using the program HKL (*18*).

The crystals of the tetragonal apoenzyme and the hemiacetal enzyme belong to space group $I4_1$ with the following unit cell dimensions: $a = 119.6$ Å and $c = 158.6$ Å and $a = 120.8$ Å and $c = 157.7$ Å, respectively. Two subunits are present per asymmetric unit. The crystal of monoclinic apoenzyme belongs to space group $C2$ with the following unit cell dimensions: $a = 81.8$ Å, $b = 134.6$ Å, $c = 68.2$ Å, and $\beta = 106.1°$. Although the NAD^+ soaking did not change the space group, the unit cell dimensions changed: $a = 85.5$ Å, $b = 134.5$ Å, $c = 67.3$ Å, and $\beta = 107.9°$. Two subunits are present per asymmetric unit. The data collection statistics are shown in Table 1.

Structure Determination and Refinement. The structure of tetragonal apo-GAPDH was determined by the MAD method. This method gave an independent verification of GAPDH in the NAD^+-free state because it was known that the crystallographic studies of the apoenzyme from mesophilic organisms were hampered by the protein instability (*19*). The automated program SOLVE was used to scale the integrated

Table 2: Refinement Statistics

	tetragonal crystal forms		monoclinic crystal forms	
	apoenzyme	hemiacetal enzyme	apoenzyme	holoenzyme
refinement				
resolution (Å)	20−2.5	20−2.5	20−2.0	20−2.0
R_{free}[a]	0.241	0.258	0.281	0.292
R_{work}[b]	0.189	0.198	0.206	0.224
no. of reflections [$F > 2\sigma(F)$]	36600	34723	39405	39909
no. of protein atoms	4976	4976	4976	4976
no. of nonprotein atoms		20		88
no. of water molecules	207	241	230	259
stereochemistry				
rmsd for bond lengths (Å)	0.008	0.008	0.008	0.010
rmsd for bond angles (deg)	1.373	1.376	1.385	1.421
residues in the Ramachandran plot				
most favored regions (%)	83.6	81.8	84.6	84.6
additional allowed regions (%)	15.9	17.4	14.5	14.4
generously allowed regions (%)	0.5	0.7	0.9	0.9

[a] R_{free} is equivalent to R_{work} except that it concerns the 5% of the total reflections set aside for an unbiased test of the progress of refinement. [b] $R_{work} = \Sigma||F_{obs}| - |F_{calc}||/\Sigma|F_{obs}|$, where $|F_{obs}|$ and $|F_{calc}|$ are observed and calculated structure factor amplitudes, respectively.

data sets, to calculate Patterson functions, to find and optimize the 14 selenium atom sites, and to calculate protein phases (*20*). The initial electron density map was improved by the NCS-averaging method using the program DM (the CCP4 suite) (*21*). The atomic model was built using the graphics program O (*22*). The model was refined against the data set collected at the wavelength corresponding to the inflection point of the selenium edge in the program XPLOR (*23*). During refinement, NCS restraints were not imposed. The final structure contains two complete protein subunits (330 residues each), and its refinement statistics are listed in Table 2.

The structure of hemiacetal GAPDH was determined by using XPLOR (*20*) to refine the final model of the tetragonal apoenzyme against the hemiacetal enzyme data. Refinement was performed without imposing NCS restraints. The difference electron density map [$F_{o(\text{hemiacetal enzyme})} - F_{c(\text{tetragonal apoenzyme})}$] indicated that residues 207−212, which form a strand−loop−helix structure, had moved, and the region was appropriately adjusted. The difference map also exhibited other strong positive density connected to the SH group of Cys149. GAP changed into a hemiacetal intermediate was fitted to this electron density. After the final refinement, both of the two hemiacetal intermediates in the asymmetric unit could be superimposed with an rms difference of 0.023 Å. The electron density map of the hemiacetal intermediate is shown in Figure 1a. The final refinement statistics are listed in Table 2.

The structures of monoclinic apo-GAPDH and holo-GAPDH were determined by molecular replacement using a subunit of the tetragonal apoenzyme as a search model. The program XPLOR (*23*) was used for the rotation and translation searches. The two best solutions for the rotation matrix corresponded to two subunits of GAPDH present in the asymmetric unit. The first translation search, restricted to the *x* and *z* dimensions, was carried out after the search model coordinates had been rotated according to one of the two best rotation matrices. The translation function clearly identified a solution that was 23σ above the next highest peak. This solution corresponds to the position of the first subunit of GAPDH. The second translation search, performed after the noncrystallographic symmetry had been applied to the coordinates of the first subunit, yielded a solution corresponding to the position of the second subunit. When the relative translation between the first and second subunits had been determined, the model containing both subunits was subjected to rigid body refinement; the two subunits were considered to be independent rigid structures. The rigid body refinement led to an *R* factor of 30.0% at a resolution between 6.0 and 4.0 Å. Several iterations of refinement and model building improved the monoclinic apoenzyme structure. This refined structure was subjected to further refinement against diffraction data of the holoenzyme. The cofactor NAD^+ was then fit to the corresponding difference electron density calculated by using coefficients $F_{o(\text{holoenzyme})} - F_{c(\text{monoclinic apoenzyme})}$. The final refinement statistics for both the monoclinic apoenzyme structure and the holoenzyme structure are listed in Table 2. The superposition of the two refined NAD^+ molecules in the asymmetric unit gave an rms difference of 0.11 Å, suggesting that the refined NAD^+ models in the two subunits are almost identical. The refined NAD^+ model with its electron density is shown in Figure 1b.

RESULTS

Overall Structure. All the structures of GAPDH presented here contain Se-Met. The structures of monoclinic apo-GAPDH and holo-GAPDH and those of tetragonal apo-GAPDH and hemiacetal GAPDH consist of a homotetramer whose subunits designated O, P, Q, and R are arranged with local 222 symmetry on three molecular axes designated P, Q, and R (for nomenclature, see ref *24*) (Figure 2). The asymmetric unit for the monoclinic apoenzyme and holoenzyme structures comprises two subunits, O and Q, whereas in the structures of the tetragonal apoenzyme and hemiacetal enzyme, the asymmetric unit comprises two subunits, Q and R. Superposition of subunits O and Q for the monoclinic apoenzyme and the holoenzyme results in rms differences of 0.298 and 0.291 Å, respectively. For the tetragonal apoenzyme and hemiacetal enzyme, the rms differences between subunits Q and R are 0.116 and 0.221 Å, respectively. The fact that these values are below the estimated coordinate errors indicates that there are no dramatic differences between the two subunits of the crystal asymmetric

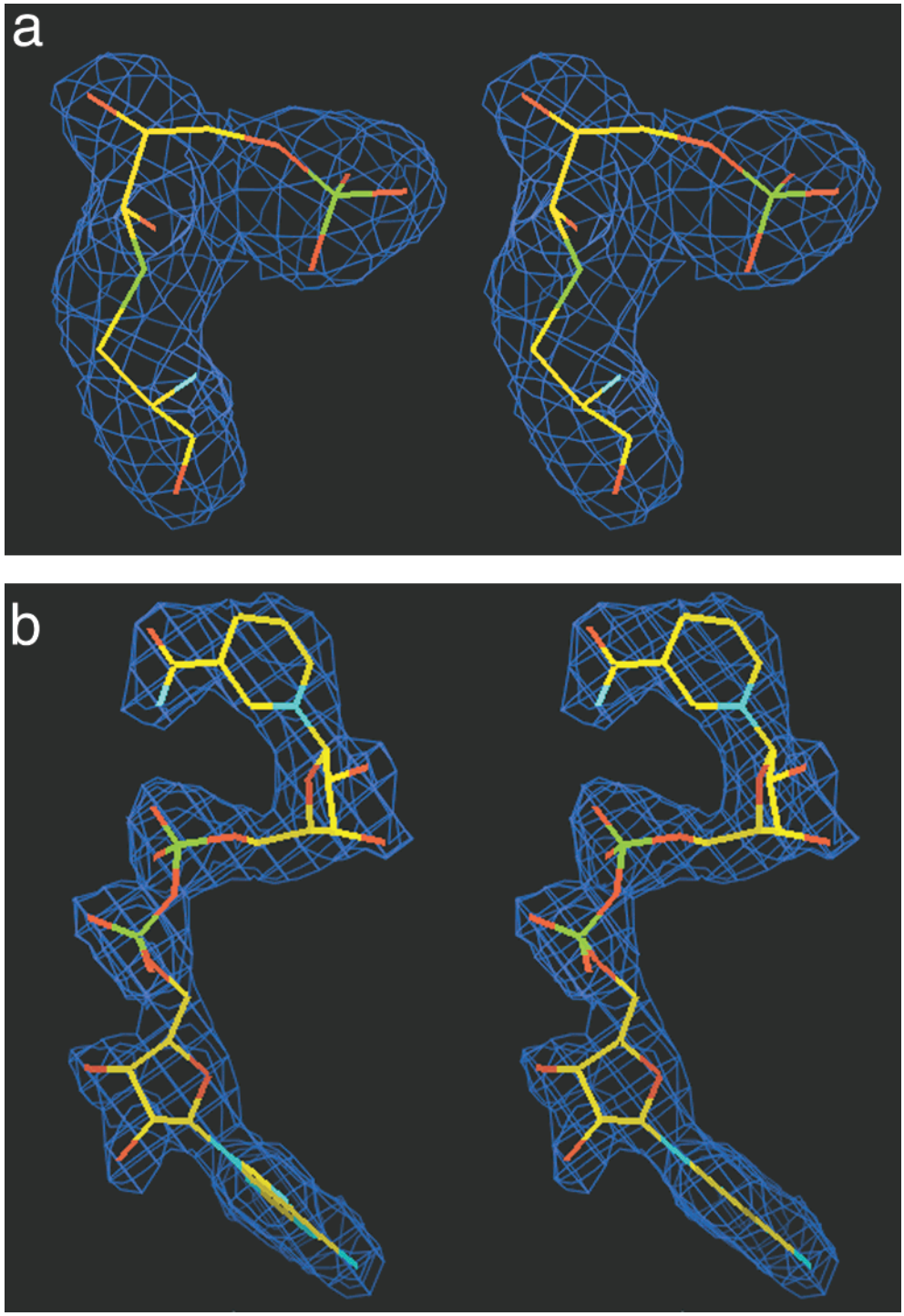

FIGURE 1: Stereoview of electron density maps. (a) Hemiacetal intermediate of the GAP−Cys149 complex of subunit O. (b) NAD^+ cofactor of subunit O. After exclusion of the hemiacetal intermediate or NAD^+, electron density maps were computed using the coefficients $F_o - F_c$ and contoured at 3σ. Carbon atoms are shown in yellow, nitrogen atoms in cyan, oxygen atoms in red, and phosphorus atoms in green, and the sulfur atom of Cys149 is in light green. This figure was produced with the program XtalView (*34*).

unit in all four structures. Structural differences of monoclinic and tetragonal apoenzymes are also analyzed. When subunits O and Q of the monoclinic apoenzyme are individually superimposed on subunits Q and R of the tetragonal apoenzyme, the average rms difference of Cα atoms is 0.34 Å. This low rms difference value suggests that the overall structures of these two apoenzymes are comparable to each other.

In all four structures of GAPDH reported here, each subunit is composed of two domains: the N-terminal NAD^+-binding domain (residues 0−147 and 311−330) and the C-terminal catalytic domain (residues 148−310) (for numbering of the amino acid sequence, see ref *25*). The NAD^+-binding domain has an α/β dinucleotide-binding fold. The catalytic domain folds into an eight-stranded, mixed parallel β-sheet, in which the strands are connected by either short loops or α-helices.

Structural Comparison of Monoclinic Apo-GAPDH and Holo-GAPDH. A superposition of the two structures shows that the main differences occur in the NAD^+-binding domain.

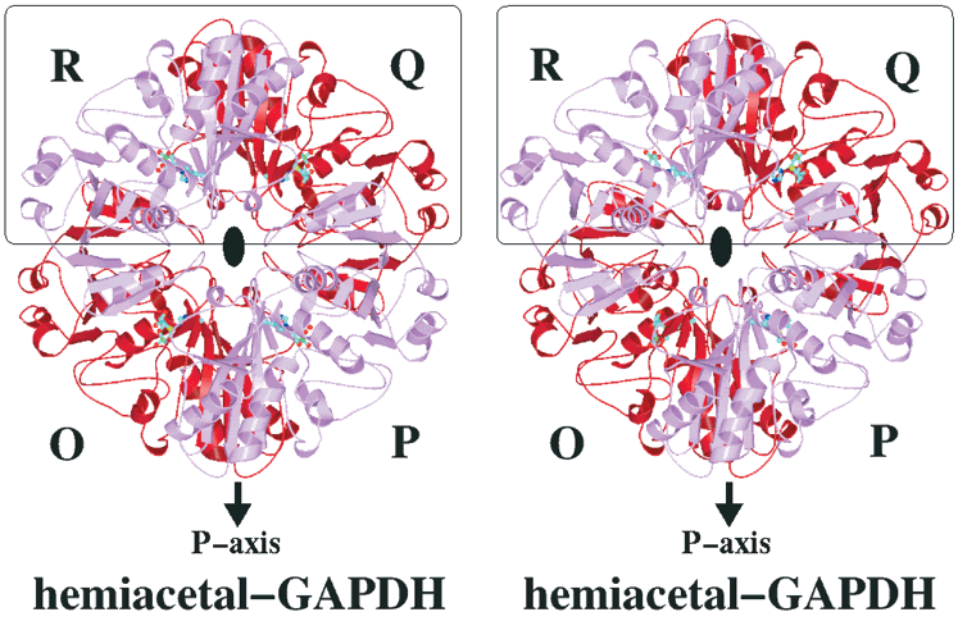

FIGURE 2: Overall view of the hemiacetal enzyme structure in a ribbon representation. All four subunits are shown. Subunits Q and R of the asymmetric unit in the boxed area are colored red and pink, respectively, and their symmetry-related subunits O and P are also colored red and pink, respectively. The view is along the Q axis with the P axis vertical. This figure was produced with the program MOLSCRIPT (*35*).

Thus, the catalytic domains superimpose with an rms difference of 0.26 Å, whereas the NAD^+-binding domains superimpose with an rms difference of 0.38 Å. The actual structural change induced by NAD^+ binding increases the H-bond distance between the thiol group of Cys149 and the Nϵ nitrogen of His176 at the active site from 3.41 to 3.53 Å (data not shown). This observation is of interest because the distance between the corresponding residues in the *B. stearothermophilus* structure decreases after NAD^+ binding to form an H-bond (*16*).

In the holoenzyme structure, the cofactor NAD^+ is bound to GAPDH in an extended conformation (Figure 1b) similar to the NAD^+ conformation found in the GAPDH structures from *E. coli* and other organisms (*26*). NAD^+ sits in a groove of the NAD^+-binding domain (Figure 3). The backbone nitrogens of residues 10 and 11 are within H-bonding distance of the oxygens in the pyrophosphate moiety of NAD^+, and the backbone nitrogens of residues 7, 9, and 12 have water-mediated interactions with the same oxygens. However, in the monoclinic apoenzyme structure, the absent pyrophosphate moiety of NAD^+ is replaced with three water molecules.

In the holoenzyme structure, binding of the adenine moiety of NAD^+ rearranges the carboxyl oxygens of the Asp32 side chain to form two H-bonds with the 2′- and 3′-hydroxyl groups of the adenine sugar, whereas in the monoclinic apoenzyme structure, the Asp32 side chain is exposed to solvent. In the holoenzyme structure, the loop containing Arg77 is also moved toward the adenine base so that the backbone nitrogen of Arg77 can be within H-bonding distance of N6 of the adenine base. Similarly, the movement of the Asn6 side chain results in a water-mediated interaction with N1 of the adenine base. Strikingly, the Leu33 side chain has been displaced so that its distance to the adenine base for forming a van der Waals bond is 3.8 Å.

Less rearrangement of protein residues at the nicotinamide-binding site is found. In the holoenzyme structure, the backbone oxygen of Glu94, the backbone nitrogen of Gly97, and the hydroxyl group of Thr119 form water-mediated interactions with the 3′-hydroxyl group of the nicotinamide sugar. The side chain nitrogen of Asn313 is within H-bonding distance of O7 of the nicotinamide base. The backbone oxygen of Thr178 and Pro235, the backbone nitrogen of Ala180, and the carboxyl group of Glu314 interact with N7 of the nicotinamide base by means of water molecules. Side chains of residues Ile11 and Tyr317 form a van der Waals contact with the nicotinamide base. In addition to these interactions between the cofactor and the protein, there is also internal polar interaction within the cofactor. One of the pyrophosphate oxygens forms an H-bond with N7 of the nicotinamide base.

GAP-Binding Site. Compared to the tetragonal apoenzyme, the structure of the hemiacetal enzyme exhibits an altered conformation for the strand−loop−helix portion spanning residues 207−212 (Figure 4). The average *B* factor of the residues in this region is 47.8 $Å^2$, whereas that of the entire protein is 36.3 $Å^2$. The electron densities of the side chains within the strand−loop−helix portion are poorly defined, which supports the flexibility of this region. The altered conformation of the strand−loop−helix portion brings the residues that line the P_i site closer to catalytic residue Cys149. A similar movement was observed with the corresponding strand−loop−helix structure of the holoenzyme from *L. mexicana* (*10*, *11*) when it was compared to that of holoenzymes from American lobster, human, *B. stearothermophilus* and *T. brucei*. The authors suggested that the observed movement of the strand−loop−helix structure of the *L. mexicana* holoenzyme was due to the change of the crystallization counterion from sulfates to phosphates. However, the strand−loop−helix structure of the *Th. maritima* holoenzyme, compared to the *B. stearothermophilus* apoenzyme, exhibited the altered conformation, although the crystals of both enzymes were grown in a high concentration of ammonium sulfate (*7*). The movement of the strand−

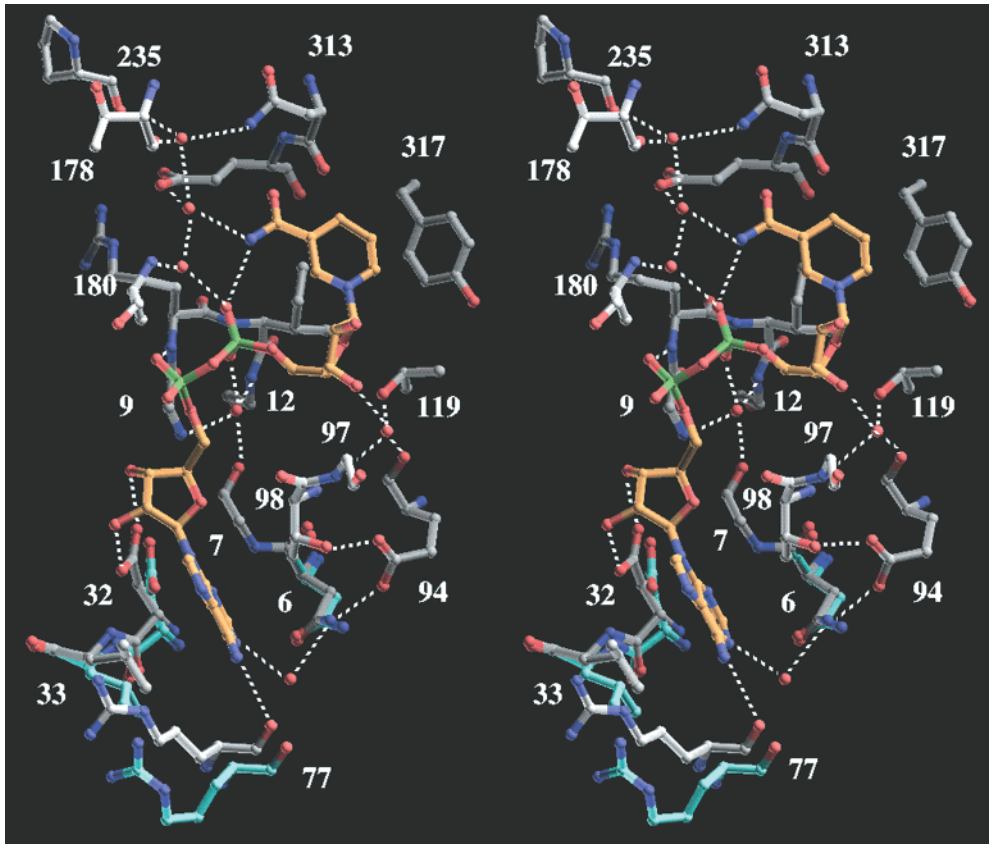

FIGURE 3: Stereoview of NAD^+ cofactor binding. Hydrogen bonding interactions are represented by dotted lines. Carbon atoms are shown in yellow for the NAD^+ cofactor, gray for the holoenzyme, and cyan for the monoclinic apoenzyme. Nitrogen atoms are shown in light blue, and other atom colors are as shown in Figure 1. For the monoclinic apoenzyme, residues 6, 32, 33, and 77 that interact with the adenine moeity of NAD^+ are shown and other residues are not shown for clarity. This figure was produced with the program O (*22*).

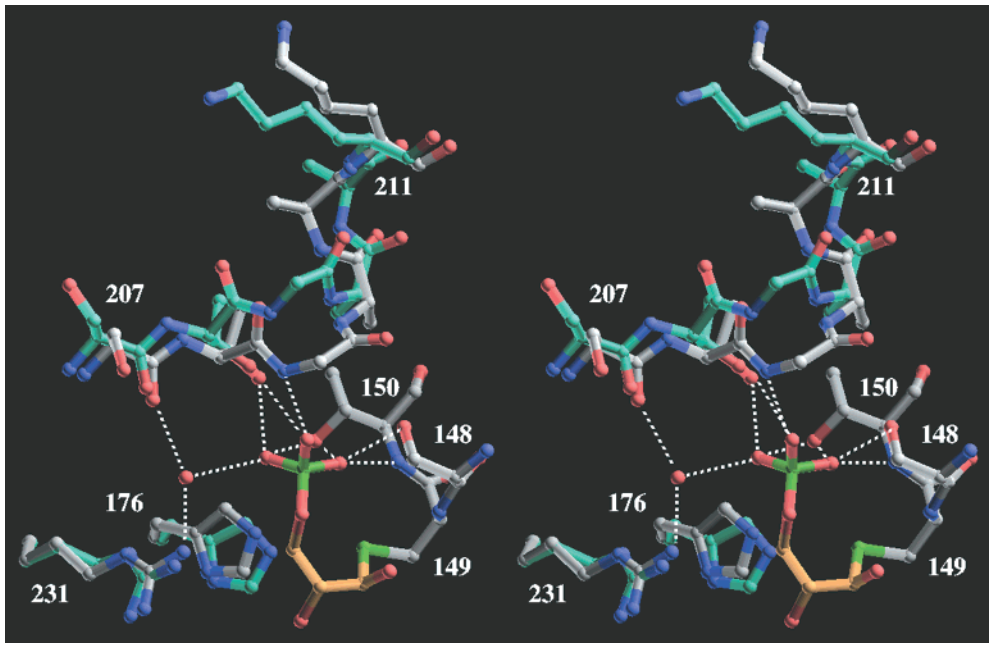

FIGURE 4: Stereoview of GAP substrate binding. Hydrogen bonding interactions are represented by dotted lines. Carbon atoms are shown in yellow for the GAP substrate, gray for the hemiacetal enzyme, and cyan for the tetragonal apoenzyme. Nitrogen atoms are shown in light blue, and other atom colors are as shown in Figure 1. For clarity, residues 148−150 of the tetragonal apoenzyme are not depicted. This figure was produced with the program O (*22*).

loop−helix structure was also observed in the Chinese lobster holoenzyme with the carboxymethylated active site, compared to the same holoenzyme with the unmodified active site (*3*). Furthermore, the strand−loop−helix structure of the *Thr. aquaticus* holoenzyme, bound with neither sulfates nor phosphates (*8*), did not exhibit the movement. Instead, it adopted a conformation similar to that of the *E. coli* tetragonal apoenzyme (data not shown). This observation suggests that the presence of the hemiacetal intermediate as well as the binding of phosphates may be required to cause

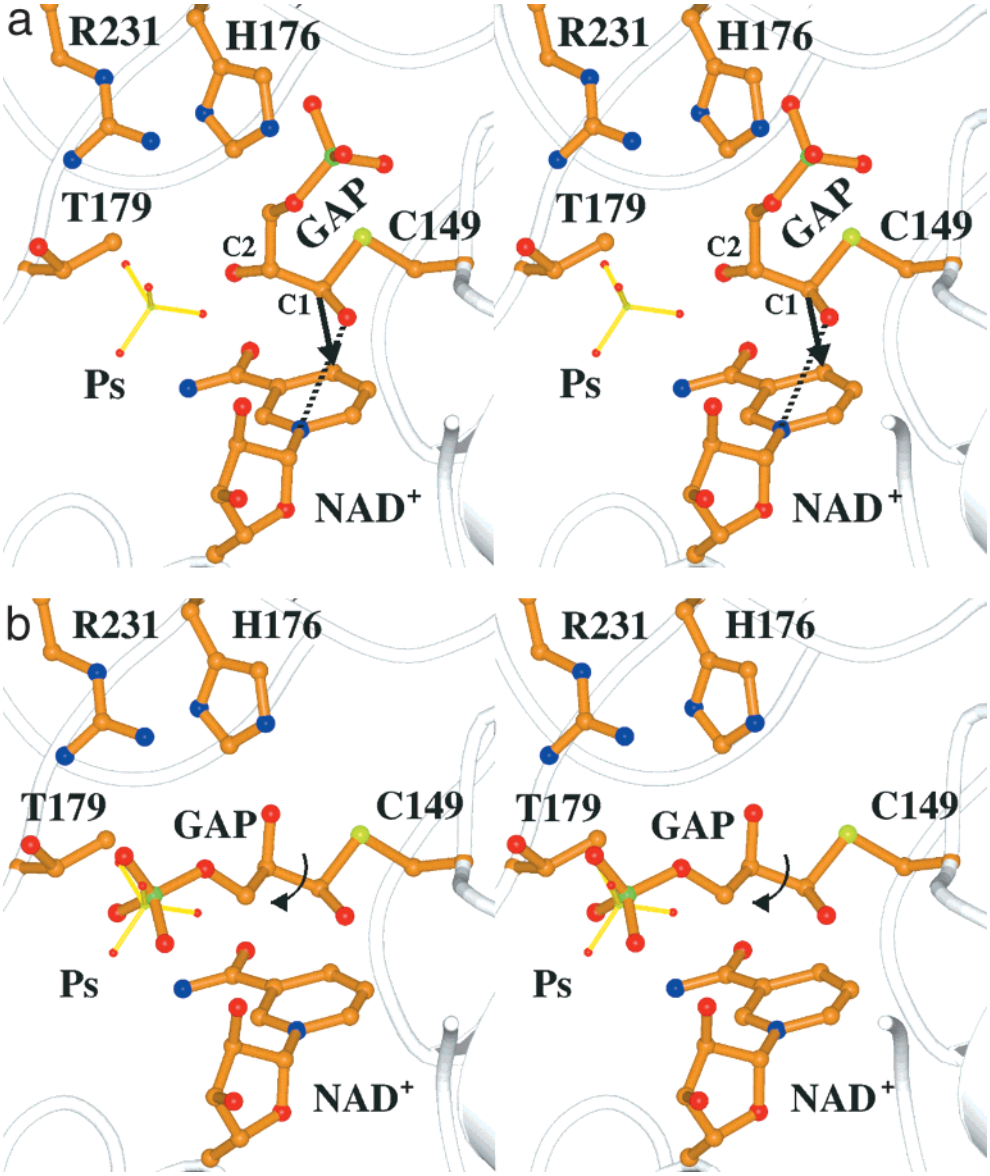

FIGURE 5: Closeup stereoview of the active site of GAPDH after the NAD^+ cofactor of the holoenzyme is overlaid onto the structure of the hemiacetal enzyme. Carbon atoms are shown in brown, nitrogen atoms in blue, oxygen atoms in red, and phosphorus atoms in green, and the sulfur atom of Cys149 is in light green. (a) The location of the P_s site is indicated by a sulfate ion that is present in *B. stearothermophilus* GAPDH (PDB code 1gd1). The sulfur atom of the sulfate ion is shown in green. The hemiacetal intermdediate is bound with its phosphate group in the new P_i site. The proposed interaction between the oxyanion at C1 of GAP and N1 of NAD^+ is represented by a dotted line. The arrow shows direct hydride transfer from C1 of GAP to C4 of NAD^+. (b) The hemiacetal intermediate bound with its phosphate group in the P_s site. The curved arrow shows the rotation around the bond between C1 and C2 which brings the phosphate group of the hemiacetal intermediate from the new P_i site to the P_s site. Please note that the depicted NAD^+ is the first cofactor to which a hydride ion is transferred. This figure was produced with the program MOLSCRIPT (*35*).

the conformational change of the strand−loop−helix structure.

The GAP molecule binds to the catalytic domain with its C3 phosphate making a number of specific interactions (Figure 4). Distances of the side chain hydroxyl groups of Ser148, Thr150, and Thr208 and the backbone nitrogens of Thr150 and Gly209 form H-bonds with the phosphate O4P and O2P oxygens. The distances between the atoms involved in these H-bonds are 2.9, 2.5, 2.7, 2.8, and 2.6 Å, respectively. The guanidinium group of Arg231 forms a water-mediated interaction with the phosphate O4P oxygen. Finally, the side chain of His176 moves closer to the C3 phosphate, and its imidazole group appears to partially compensate for the negative charge at the C3 phosphate of GAP. The difference electron density map clearly shows that hemiacetal C1 and C2 of GAP both adopt an *R* configuration (Figure 1a). As a result, the hydroxyl group of C1 points away from the hydroxyl group of C2 to adopt a trans conformation. The *R* configuration at C2 indicates that the bound GAP is D-GAP, and this is consistent with the fact that yeast GAPDH has 3.3-fold higher affinity for D-GAP than for L-GAP (*27*). In the case of L-GAP, C2 has an *S* configuration, and in the hemiacetal form, both hydroxyl groups point in the same direction to adopt a cis conformation. The distance between the two hydroxyl groups is close enough to allow an H-bond interaction, but the angle between them makes the H-bond interaction unfavorable. This suggests that the lower energy associated with the trans conformation of the hemiacetal intermediate of D-GAP makes its use by GAPDH more likely.

DISCUSSION

NAD^+-Induced Structural Changes. We have shown that the structural differences between *E. coli* monoclinic apo-GAPDH and holo-GAPDH exist primarily in the NAD^+-binding domain. The differences are more prominent at the adenine-binding site and less so at the nicotinamide-binding site. Similar structural changes have been observed for other GAPDHs and were suggested to produce a rearrangement of the active site residues that increases the nucleophilicity of the cysteine residue involved in catalysis. In the *B. stearothermophilus* holoenzyme, the NAD^+-induced structural changes shorten the distance between Cys149 and His176 at the active site to form an H-bond between them (*16*). This H-bonding interaction has been suggested to increase the nucleophilicity of the catalytic residue Cys149 to facilitate the formation of a hemiacetal intermediate in the oxidation step. However, in the *E. coli* monoclinic apoenzyme structure, these two active site residues are already near enough to allow an H-bond and to create a reactive thiol group. Furthermore, NAD^+ binding actually causes a slight increase in the H-bonding distance. Therefore, we conclude that the binding of NAD^+ to the *E. coli* enzyme is not associated with changes in the catalytic state of the protein.

GAP Binding. The structure reported here provides the first view of the hemiacetal intermediate of the GAP−enzyme complex at atomic resolution. The hydrophilic pocket, called the P_i site, is the primary binding site for the C3 phosphate of GAP. This observation is supported by mutagenesis studies in which changes in the residues lining the original P_i site, but not in those lining the P_s site, cause a dramatic reduction in the extent of NADH formation (*28*, *29*). Also, the C3 phosphate of glycidol 3-phosphate is known to bind at the P_i site (*6*).

Our results agree well with the flip-flop model proposed for the binding of GAP (*6*). The new P_i site can be incorporated into this model in the following way. The C3 phosphate of GAP initially binds to the P_i site during the formation of the hemiacetal intermediate (Figure 5a). Then, the C3 phosphate flips from the new P_i site to the P_s site before the hydride transfer (Figure 5b). The side chain of the bound GAP has a *B* factor of 49.9 Å^2, which is much higher than the average *B* factor of 36.3 Å^2 for the surrounding proteins. This supports a scheme in which the flexible GAP can readily flip its phosphate group to the P_s site. However, it should be noted that the structure of the hemiacetal enzyme is free of NAD^+ which results in an incomplete P_s site. The complete P_s site is formed by the protein residues and the C2 hydroxyl group of the nicotinamide sugar of NAD^+ (*6*). When the ternary complex structure containing both GAP and NAD^+ is determined, it will provide a description of the complete P_s site and will reveal a true binding site for GAP.

Reaction Mechanism. The formation of the hemiacetal intermediate is preceded by a tetrahedral transition state, which contains the negatively charged oxygen at C1 of GAP. When we superimpose the structures of the holoenzyme and the hemiacetal enzyme, the hydroxyl group at hemiacetal C1 of GAP and the nicotinamide base are close to one another (Figure 5a). During the tetrahedral transition state, the oxyanion at hemiacetal C1 of GAP could interact with the formal positive charge on N1 of the nicotinamide base. This could stabilize the tetrahedral transition state. A similar mechanism has been proposed for stabilizing the tetrahedral transition states of serine and cysteine proteinases in which two hydrogen bonds are provided from the protein to the oxyanion (*30*, *31*). Mutagenesis studies of *E. coli* GAPDH show that His176 plays a role in stabilizing the tetrahedral transition state and as a base catalyst for facilitating hydride transfer (*32*, *33*). These studies are not consistent with our proposal that the cofactor NAD^+ stabilizes the transition state. In the structure of the hemiacetal enzyme, His176 is involved in binding the phosphate group of GAP (Figure 4), suggesting that the role of His176 is limited to activating the nucleophilicity of Cys149 in catalysis.

ACKNOWLEDGMENT

Research carried out in part at the National Synchrotron Light Source, Brookhaven National Laboratory, which is supported by the U.S. Department of Energy, Division of Materials Sciences and Division of Chemical Sciences. We thank Drs. Zbgniew Dauter and Rajashankar K. R. for their help and advice with MAD diffraction data collection on beamline X9B. We thank Drs. Stephen White and Enrico DiGiammarino for their helpful suggestions and comments in writing the manuscript and Dayna Baker for her help in preparing the manuscript.

REFERENCES

1. Harris, J. I., and Waters, M. (1976) in *The Enzymes* (Boyer, P. D., Ed.) pp 1−49, Academic Press, New York.
2. Moras, D., Olsen, K. W., Sabesan, M. N., Buehner, M., Ford, G. C., and Rossmann, M. G. (1975) *J. Biol. Chem. 250*, 9137−9162.
3. Song, S., Li, J., and Lin, Z. (1998) *Acta Crystallogr., Sect. D: Biol. Crystallogr. 54*, 558−569.
4. Song, S. Y., Xu, Y. B., Lin, Z. J., and Tsou, C. L. (1999) *J. Mol. Biol. 287*, 719−725.
5. Watson, H. C., Duee, E., and Mercer, W. D. (1972) *Nat. New Biol. 240*, 130−133.
6. Skarzynski, T., Moody, P. C., and Wonacott, A. J. (1987) *J. Mol. Biol. 193*, 171−187.
7. Korndorfer, I., Steipe, B., Huber, R., Tomschy, A., and Jaenicke, R. (1995) *J. Mol. Biol. 246*, 511−521.
8. Tanner, J. J., Hecht, R. M., and Krause, K. L. (1996) *Biochemistry 35*, 2597−2609.
9. Duee, E., Olivier-Deyris, L., Fanchon, E., Corbier, C., Branlant, G., and Dideberg, O. (1996) *J. Mol. Biol. 257*, 814−838.
10. Kim, H., Feil, I. K., Verlinde, C. L., Petra, P. H., and Hol, W. G. (1995) *Biochemistry 34*, 14975−14986.
11. Kim, H., and Hol, W. G. (1998) *J. Mol. Biol. 278*, 5−11.
12. Vellieux, F. M., Hajdu, J., and Hol, W. G. (1995) *Acta Crystallogr., Sect. D: Biol. Crystallogr. 51*, 575−589.
13. Vellieux, F. M., Hajdu, J., Verlinde, C. L., Groendijk, H., Read, R. J., Greenhough, T. J., Campbell, J. W., Kalk, K. H., Littlechild, J. A., and Watson, H. C. (1993) *Proc. Natl. Acad. Sci. U.S.A. 90*, 2355−2359.
14. Souza, D. H., Garratt, R. C., Araujo, A. P., Guimaraes, B. G., Jesus, W. D., Michels, P. A., Hannaert, V., and Oliva, G. (1998) *FEBS Lett. 424*, 131−135.
15. Murthy, M. R., Garavito, R. M., Johnson, J. E., and Rossmann, M. G. (1980) *J. Mol. Biol. 138*, 859−872.
16. Skarzynski, T., and Wonacott, A. J. (1988) *J. Mol. Biol. 203*, 1097−1118.
17. Isupov, M. N., Fleming, T. M., Dalby, A. R., Crowhurst, G. S., Bourne, P. C., and Littlechild, J. A. (1999) *J. Mol. Biol. 291*, 651−660.
18. Otwinowski, Z., and Minor, W. (1997) *Methods Enzymol. 276A*, 307−326.

19. Harris, J. I., Hocking, J. D., Runswick, M. J., Suzuki, K., and Walker, J. E. (1980) *Eur. J. Biochem. 108*, 535−547.
20. Terwilliger, T., and Berendzen, J. (1999) *Acta Crystallogr., Sect. D: Biol. Crystallogr. 55*, 501.
21. Collaborative Computational Project No. 4 (1994) *Acta Crystallogr., Sect. D: Biol. Crystallogr. 50*, 760.
22. Jones, T. A., Zou, J. Y., Cowan, S. W., and Kjeldgaard, M. (1991) *Acta Crystallogr., Sect. A: Found. Crystallogr. 47*, 110−119.
23. Brünger, A. T. (1992) *X-PLOR, a system for X-ray crystallography and NMR*, version 3.1, Yale University Press, New Haven, CT.
24. Buehner, M., Ford, G. C., Moras, D., Olsen, K. W., and Rossmann, M. G. (1974) *J. Mol. Biol. 82*, 563−585.
25. Branlant, G., and Branlant, C. (1985) *Eur. J. Biochem. 150*, 61−66.
26. Bernstein, F. C., Koetzle, T. F., Williams, G. J., Meyer, E. F., Jr., Brice, M. D., Rodgers, J. R., Kennard, O., Shimanouchi, T., and Tasumi, M. (1977) *Eur. J. Biochem. 80*, 319−324.
27. Byers, L. D. (1978) *Arch. Biochem. Biophys. 186*, 335−342.
28. Corbier, C., Michels, S., Wonacott, A. J., and Branlant, G. (1994) *Biochemistry 33*, 3260−3265.
29. Michels, S., Rogalska, E., and Branlant, G. (1996) *Eur. J. Biochem. 235*, 641−647.
30. Polgar, L., and Halasz, P. (1982) *Biochem. J. 207*, 1−10.
31. Steitz, T. A., and Shulman, R. G. (1982) *Annu. Rev. Biophys. Bioeng. 11*, 419−444.
32. Soukri, A., Mougin, A., Corbier, C., Wonacott, A., Branlant, C., and Branlant, G. (1989) *Biochemistry 28*, 2586−2592.
33. Talfournier, F., Colloc'h, N., Mornon, J. P., and Branlant, G. (1998) *Eur. J. Biochem. 252*, 447−457.
34. McRee, D. E. (1998) *XtalView*, version 3.2.1, The Scripps Research Institute, La Jolla, CA.
35. Kraulis, P. J. (1991) *J. Appl. Crystallogr. 24*, 946−950.

BI9927080